# Ultralong-range energy transfer by interatomic Coulombic decay in an extreme quantum system

Nicolas Sisourat[1], Nikolai V. Kryzhevoi[1], Přemysl Kolorenč[2], Simona Scheit[3], Till Jahnke[4] and Lorenz S. Cederbaum[1]*

When an atom is electronically excited, it relaxes by emitting a photon or an electron. These carry essential information on the electronic structure of their emitter. However, if an atom is embedded in a chemical environment, another ultrafast non-radiative decay process called interatomic Coulombic decay (ICD) can become operative[1]. As ICD occurs only in the presence of neighbours, it is highly sensitive to that environment. Therefore, it has the potential to become a powerful spectroscopic method to probe the close environment of a system. ICD has been observed experimentally in van der Waals clusters[2-5] as well as in hydrogen-bonded systems[6-8]. A key feature of ICD is that the excited atom can transfer its excess energy to its neighbours over large distances. The giant extremely weakly bound helium dimer is a perfect candidate to investigate how far two atoms can exchange energy. We report here that the two helium atoms within the dimer can exchange energy by ICD over distances of more than 45 times their atomic radius. Moreover, we demonstrate that ICD spectroscopy can be used for imaging vibrational wavefunctions of the ionized–excited helium dimer.

The existence of the helium dimer had been discussed for decades before it was observed experimentally[9]. It is an extreme quantum system: it is the most weakly bound system in nature, with a binding energy of about 10^{-7} eV (≈ 1.1 mK) and a very large average bond length of roughly 52 Å (ref. 10). The huge separation between the two helium atoms within the dimer makes the study of ultralong-range energy transfer and ultralong-range nuclear dynamics possible. Initially, ICD was predicted to occur after ionization of an inner-valence-shell electron of an atom or a molecule embedded in an environment. The excited system relaxes electronically by transferring, through a virtual photon mechanism[11], its excess energy to a neighbour and ionizing it. However, helium atoms have no inner-valence electrons and standard ICD cannot occur. Nevertheless, it was suggested[12] that a new kind of ICD process is possible in a helium dimer. After simultaneous ionization and excitation of one helium atom within the dimer, the energy stored by this excited ion suffices to ionize the neighbouring neutral helium atom. The excited ion relaxes by ICD to He$^+$(1s) and the neutral helium is ionized to He$^+$(1s) as well and emits the ICD electron. The resulting two He$^+$(1s) then undergo a Coulomb explosion and fly apart. In short,

$$\text{He–He} \xrightarrow{h\nu} \text{He}^{+*}\text{–He} + e_{ph}^- \xrightarrow{ICD} \text{He}^+ + \text{He}^+ + e_{ph}^- + e_{ICD}^-$$
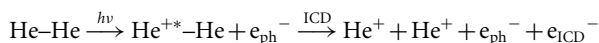
We consider in this report a photon-energy range in which only

He$^+$(n) up to $n = 2$ can be reached. Consequently, to describe the ICD process only molecular states of He$_2^+$ which correspond to He$^+$($n = 2$)–He states have to be taken into account. The potential-energy curves (PECs) are shown in Fig. 1. We label the electronic states by their configuration term and the atomic state of the excited He$^+$ at infinite interatomic distance. Two kinds of PEC are identified. The first kind is related to so-called $2p$ states denoted $^2\Sigma_g{}^+$: $2p_z$, $^2\Sigma_u{}^+$: $2p_z$, $^2\Pi_u$: $2p_{x,y}$ and $^2\Pi_g$: $2p_{x,y}$, and exhibits minima around 2 Å, which are deep enough to support eight vibrational states each. Depending on the vibrational quantum number, the binding energy of these vibrational states varies between 200 meV and 2 µeV and their mean interatomic distance is within the range of 2–27 Å. The second kind is related to so-called $2s$ states denoted $^2\Sigma_g{}^+$: $2s$, $^2\Sigma_u{}^+$: $2s$, and possesses shallower minima centred around 5 Å which support only two vibrational states each. The binding energy of the latter is between 310 and 4 µeV and their mean interatomic distance varies between 10 and 19 Å. All the respective electronic states can decay to He$^+$–He$^+$ singlet as well as triplet final states ($^1\Sigma_g{}^+$ and $^3\Sigma_u{}^+$). The corresponding ICD rates as a function of internuclear distance R are depicted in the top panel of Fig. 1. As seen in the figure, the ICD rates strongly depend on R; the shorter the distance between the atoms is, the faster is the ICD. The ICD rates must be compared with their corresponding radiative decay rates. The radiative decay is an atomic property of He$^+$($n = 2$) not influenced by the presence of the neutral helium. The radiative decay rate can be assumed to be constant over the relevant internuclear distance. According to the atomic spectroscopic data[13,14], the radiative lifetime of the He$^+$($2p$) states is about 100 ps and that of the He$^+$($2s$) state is 2 ms. As seen in Fig. 1, ICD is the dominant decay channel at distances below 10 Å for all the decaying electronic states. At larger distances, photon emission starts to be competitive and is largely dominant at interatomic distances above 20 Å.

The PECs and the ICD rates were used as input data to compute numerically exactly the distributions of the kinetic energy released by the two He$^+$ ions after ICD (see the Methods section below for details of the computations of these distributions, the PECs and the ICD rates). We show in Fig. 2 the kinetic-energy-release (KER) spectra for each electronic-state symmetry. For comparison we also show the distribution obtained assuming that ICD is instantaneous (sudden approximation), that is, the system decays before the produced He$^+$($n = 2$) and its neutral helium partner have time to move. The exact spectra exhibit a series of peaks in the energy range of 1–9 eV, whose intensities increase with increasing energy, whereas the spectrum obtained in the sudden
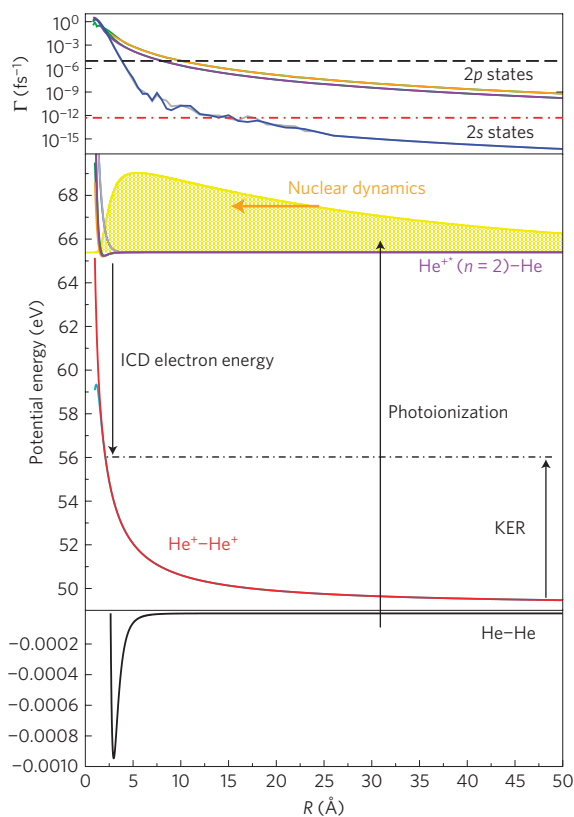
Figure 1 | *Ab initio* data relevant for ICD in He₂. Top panel, ICD rates for the decaying He$^+$($n=2$)–He states: $^2\Sigma_u^+$: $2p_z$ (green line, which is hidden behind the orange line), $^2\Sigma_g^+$: $2p_z$ (orange line), $^2\Pi_u$: $2p_{x,y}$ (purple line), $^2\Pi_g$: $2p_{x,y}$ (dark-green line, which is hidden behind the purple line), $^2\Sigma_u^+$: $2s$ (grey line) and $^2\Sigma_g^+$: $2s$ (blue line). The horizontal lines in the top panel indicate the values of the radiative decay rates for He$^+$($2s$) (red dashed–dotted line) and for He$^+$($2p$) (black dashed line). Lower panels, PECs for He-He (black line), He$^+$–He$^+$ (red and cyan lines) and He$^+$($n=2$)–He (same colour notation as in top panel) states. The nuclear wavefunction of the ground state of the dimer is shown in yellow. After photoionization of a helium atom in the dimer, the system is left in one of the He$^+$($n=2$)–He states. The excited He$^+$ relaxes by transferring its energy by ICD to ionize the neighbouring helium atom, which emits the ICD electron. The system ends in dissociative He$^+$–He$^+$ states.

Figure 2 | Partial KER spectra of the two He$^+$ ions after ICD for the different He$^+$ ($n=2$)–He electronic states decaying into singlet (dashed lines) and triplet (full lines) He$^+$–He$^+$ states. KER spectra for electronic states with the same symmetry are depicted together. Each KER spectrum is compared with that obtained within the sudden approximation (black lines). The severe failure of this approximation shows that the two atoms move over long distances during the ICD process (see the text).

approximation is structureless and decreases monotonically from 0.1 to 5 eV. The remarkable difference between these distributions demonstrates that nuclear dynamics is essential in the ICD process and that this dynamics is of an impressive quantum nature. Indeed, after the photoionization process the total nuclear wavefunction of the system in the electronic state under consideration is a linear combination of the vibrational states of this state. We calculated the lifetime of each involved vibrational state for all electronic states. The ICD lifetime of these vibrational states varies between 20 fs and 50 ps. As the characteristic vibration period of He₂$^+$ is about 300 fs, the dimer can make up to 100 vibrational cycles before it decays completely, having time to span several times the entire internuclear distance populated by these vibrational states.

Obviously, the vibrational motion of the photoionized helium dimer plays an essential role during the ICD process and we can investigate the structures observed in the KER distributions by looking at the individual vibrational wavefunctions. In the upper part of Fig. 3, we show the probability density of the main populated vibrational state ($v=7$) of the decaying $^2\Sigma_g^+$: $2p_z$ electronic state as a function of interatomic distance. The probability density of this vibrational state has maxima and minima corresponding to
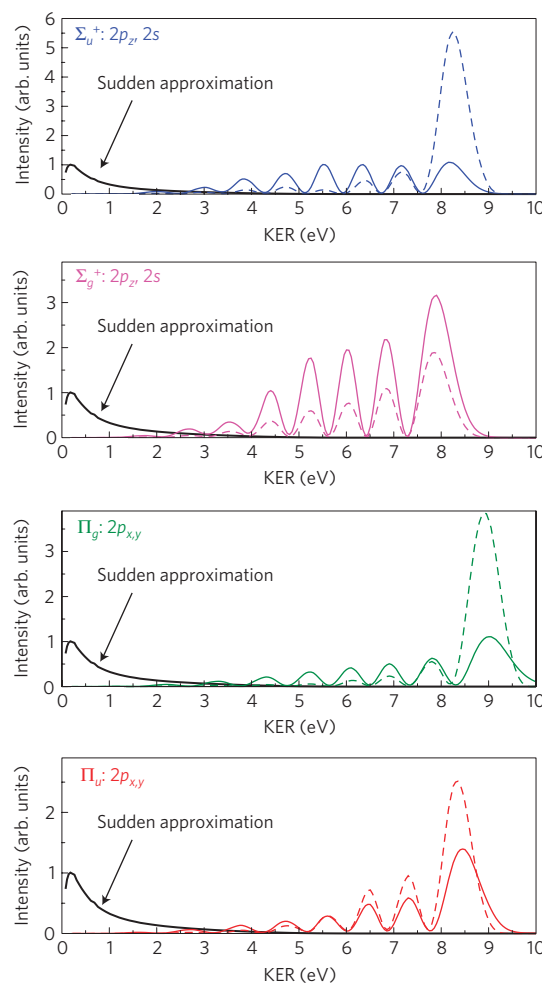
extrema and nodal structures of the vibrational wavefunction, respectively. We first compare the structures of the vibrational wavefunction with those in the KER distribution of the decaying $^2\Sigma_g^+$: $2p_z$ electronic state with the help of the well-known reflection principle[15]: the wavefunction is projected onto the final PEC and, therefore, there is a one-to-one relationship between the internuclear distance and the KER (as shown in Fig. 3). It should be noted that several additional vibrational states contribute to the KER spectrum shown, but these have small contributions. As we can see in Fig. 3, there is a clear correspondence between the appearance of nodal structures of the vibrational wavefunction and those in the KER spectrum. We conclude that the structures in the KER distribution are the fingerprints of the nodal structure of the main populated vibrational wavefunction. However, although the reflection principle succeeds in describing the positions of the minima and maxima in the KER spectrum, it fails severely in reproducing the correct relative intensities of the peaks. In Fig. 3 (upper panel), we also show the probability density of the main populated wavefunction multiplied by R^{-6}. Through the weight factor R^{-6} we take into account the decay-rate dependence predicted by the virtual-photon-transfer mechanism. It is only after this extension of the reflection principle that the relative
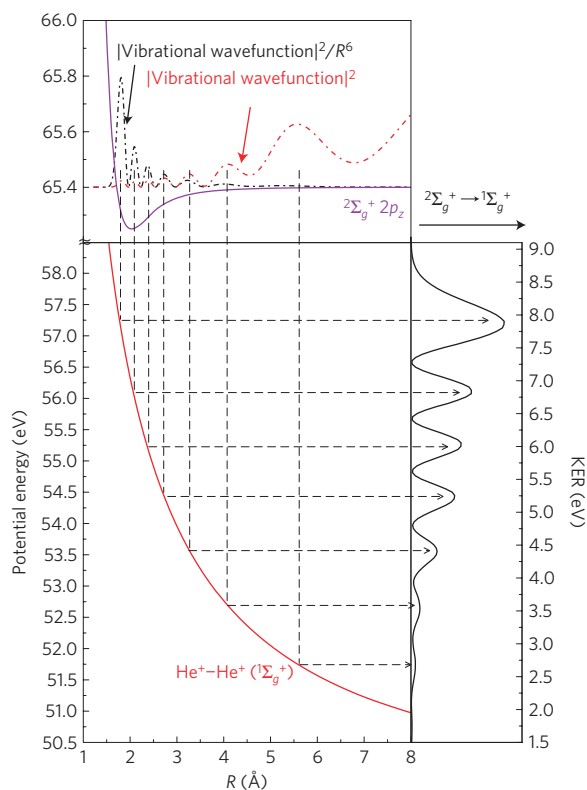
Figure 3 | Ultralong-range character of the quantum nuclear dynamics during ICD. Top panel: density probability of the most populated vibrational wavefunction of the $^2\Sigma_g^+$: $2p_z$ electronic state after photoionization of He_2 (red dashed–dotted line) and the same density probability multiplied by R^{-6} (black dashed–dotted line). The factor R^{-6} is included to take into account the decay-rate behaviour. Middle panel: PEC of the He^+–He^+ singlet final state (red line). Right panel: KER spectrum of the two He^+ ions after ICD for $^2\Sigma_g^+$: $2p_z$ decaying into the He^+–He^+ singlet final state. We show that the KER spectrum is the projection of the vibrational states weighted by R^{-6} onto the repulsive (He^+–He^+) final curve. In contrast, the commonly used reflection principle fails to reproduce the relative intensities of the peaks owing to the ultralong-range character of the energy transfer (see the text).

intensities of the peaks are also correctly reproduced. Weighting by the decay rate appropriately enhances the wavefunction at short interatomic distances and suppresses it at long distances. Obviously, the introduction of such a weight factor plays an essential role if the system is extended over large interatomic distances. The fact that the commonly used reflection principle fails to predict the KER distribution is due to the extreme extent of the ionized–excited helium dimer system and shows the ultralong-range character of the quantum dynamics of the ICD process. We have demonstrated that the KER spectrum is determined by the projection of the vibrational states onto the repulsive (He^+–He^+) final curve weighted by R^{-6} owing to the ICD-rate behaviour. This makes clear that ICD can be used to map the vibrational wavefunctions of the ionized–excited helium dimer. In particular, if we can excite specifically a vibrational state of a decaying electronic state, it is then possible to reconstruct the vibrational wavefunction from the KER distribution.

It is nowadays possible to measure the KER distribution of the two fragments of a dimer with great resolution using the COLTRIMS technique[16]. However, in the considered ICD process it is not possible yet to experimentally distinguish between the ICD processes starting from different He^+($n = 2$)–He states. Therefore, the measured KER spectrum is the sum of all partial spectra.
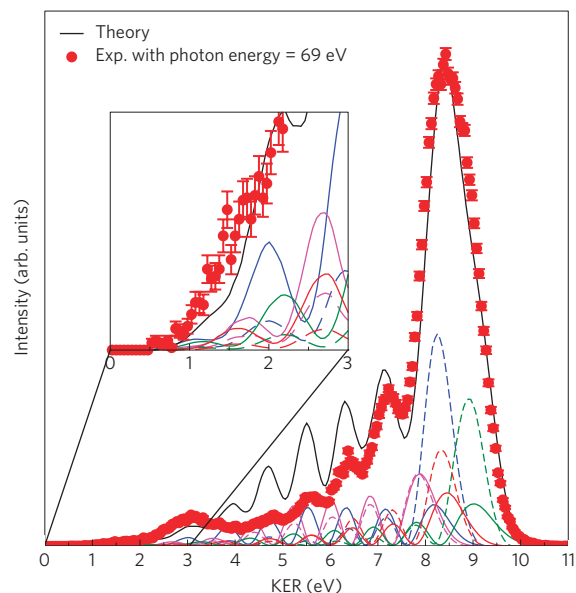

Figure 4 | Computed and measured total KER spectrum of the two He^+ after ICD. Total KER spectrum (black curve) obtained by adding all partial spectra (coloured lines below the total KER line as in Fig. 2). The experimental total KER spectrum is also shown (red dots with error bars). The error bars represent the statistical error of the measurement. The sum over all electronic states still nicely reflects the nodal structures of the participating vibrational wavefunctions found in the partial spectra. The reflection principle (see the text) makes it possible to assign a KER value to a given interatomic distance at which the ICD process takes place. The smallest significant KER is at about 1 eV (see the inset), which corresponds to an interatomic separation around 14 Å, implying that the two atoms can exchange energy over more than 45 times their atomic radius.

Nevertheless, we can show here that the sum over all electronic states still nicely reflects the structures in the partial spectra. The calculated total KER spectrum is compared with that measured (ref. 12 and Methods below) in Fig. 4. All partial spectra are shown in this figure as well. The agreement between the computed and measured KER distributions is surprisingly good for such an extreme quantum system. The total KER spectrum exhibits an intense peak at about 8.5 eV and a series of smaller peaks at lower energy, down to 1 eV. It is evident that these peaks are due to the survival of the structures showing up in the individual partial spectra and these in turn are images of the vibrational wavefunctions participating in the ICD process.

From the KER spectra, we can determine the internuclear-distance distribution over which ICD takes place. Using again the reflection principle, we can assign each KER signal to an interatomic distance. The intense peak at 8.5 eV corresponds to interatomic separation around 2 Å. Signals at smaller KER correspond to larger internuclear distances. We can see in the inset of Fig. 4 that the last observable low-KER signal is at about 1 eV, which corresponds to an internuclear distance around 14 Å. This demonstrates that energy can be transferred from one atom to another over huge distances, which correspond to more than 45 times the atomic radius. We recall that for $R > 10$ Å radiative decay becomes the main channel and this limits the observability of ICD at larger internuclear distances.

The present study shows that ICD spectroscopy can be used to explore the chemical environment of a system over large distances and is indeed a powerful tool for probing matter. From both the experimental and theoretical sides, an obvious next step is to investigate more complex systems using ICD to gather information on their structure and dynamics.

Methods

We computed fully *ab initio* the KER distributions after ICD in the helium dimer using sophisticated methods to treat the electronic structure as well as the quantum nuclear dynamics. To compute the distributions, we need the PECs of the involved electronic states and the corresponding ICD rates as functions of interatomic distance. We applied the full configuration interaction method, which is exact in the limit of a complete basis set, to compute the PECs. The accurate PEC for the electronic ground state of the helium dimer was taken from ref. 17. The decay rates were obtained for each of the decaying states by the most accurate method available: the Fano–Green function–Stieltjes technique[18,19]. The PECs and the ICD rates were used as input data to compute the KER spectra. The quantum nuclear dynamics was treated using the time-independent approach developed in ref. 20. The space spanned by the two helium atoms was discretized over a grid. Owing to the extremely large extent of the wavefunctions of He_2 involved in the ICD process, we were forced to introduce a grid of huge size, extending over more than 200 Å.

The experimental data were obtained employing Cold Target Recoil Ion Momentum Spectroscopy (COLTRIMS; ref. 16). A precooled (18 K) supersonic helium gas jet consisting of 2% helium dimers was crossed with a photon beam of monochromatized, linearly polarized photons at beamline UE112PGM2 of the BESSY synchrotron, creating a well-defined interaction volume. Charged reaction products were guided by homogenous electric and magnetic fields ($E = 12\,V\,cm^{-1}$ and $B = 10\,G$, respectively) towards two time- and position-sensitive microchannel plate detectors with delay-line position readout (see www.roentdek.com for details of the detectors). The reaction products were measured in coincidence and the data were recorded eventwise by storing the times of flight and positions of impact to a listmode file. From these measured raw data, the vector momentum of each detected particle was obtained during an offline analysis. Furthermore, the listmode technique enables us to restrict the plotted dataset to a case where momentum conservation assuming the break-up of a helium dimer is fulfilled, thus leading to nearly background-free spectra. The energy resolution of the presented KER distribution is less than 150 meV for all energies shown in Fig. 4.

References

1. Cederbaum, L. S., Zobeley, J. & Tarantelli, F. Giant intermolecular decay and fragmentation of clusters. *Phys. Rev. Lett.* **79,** 4778–4781 (1997).
2. Marburger, S., Kugeler, O., Hergenhahn, U. & Möller, T. Experimental evidence for interatomic Coulombic decay in Ne clusters. *Phys. Rev. Lett.* **90,** 203401 (2003).
3. Jahnke, T. *et al.* Experimental observation of interatomic Coulombic decay in neon dimers. *Phys. Rev. Lett.* **93,** 163401 (2004).
4. Aoto, T. *et al.* Properties of resonant interatomic Coulombic decay in Ne dimers. *Phys. Rev. Lett.* **97,** 243401 (2006).
5. Kreidi, K. *et al.* Relaxation processes following 1s photoionization and Auger decay in Ne_2. *Phys. Rev. A* **78,** 043422 (2008).
6. Aziz, E. F., Ottosson, N., Faubel, M., Hertel, I. V. & Winter, B. Interaction between liquid water and hydroxide revealed by core-hole de-excitation. *Nature* **455,** 89–91 (2008).
7. Jahnke, T. *et al.* Ultrafast energy transfer between water molecules. *Nature Phys.* **6,** 139–142 (2010).
8. Mucke, M. *et al.* A hitherto unrecognized source of low energy electrons in water. *Nature Phys.* **6,** 143–146 (2010).
9. Luo, F., McBane, G. C., Kim, G., Giese, C. F. & Gentry, W. R. The weakest bond: Experimental observation of helium dimer. *J. Chem. Phys.* **98,** 3564–3567 (1993).
10. Grisenti, R. E. *et al.* Determination of the bond length and binding energy of the helium dimer by diffraction from a transmission grating. *Phys. Rev. Lett.* **85,** 2284–2287 (2000).
11. Averbukh, V., Müller, I. B. & Cederbaum, L. S. Mechanism of interatomic Coulombic decay in clusters. *Phys. Rev. Lett.* **93,** 263002–263005 (2004).
12. Havermeier, T. *et al.* Interatomic Coulombic decay following photoionization of the helium dimer observation of vibrational structure. *Phys. Rev. Lett.* **104,** 133401 (2010).
13. Drake, G. W. F., Kwela, J. & van Wijngaarden, A. $He^+ 2p$ state lifetime by a quenching-asymmetry measurement. *Phys. Rev. A* **46,** 113–124 (1992).
14. Prior, M. H. Lifetime of the $2s$ state of He^+. *Phys. Rev. Lett.* **29,** 611–614 (1972).
15. Weber, A. O. *et al.* Complete photo-fragmentation of the deuterium molecule. *Nature* **431,** 437–440 (2004).
16. Ullrich, J. *et al.* Recoil-ion and electron momentum spectroscopy: Reaction-microscopes. *Rep. Prog. Phys.* **66,** 1463–1545 (2003).
17. Tang, K. T., Toennies, J. P. & Yiu, C. L. Accurate analytical He–He van der Waals potential based on perturbation theory. *Phys. Rev. Lett.* **74,** 1546–1549 (1995).
18. Averbukh, V. & Cederbaum, L. S. *Ab initio* calculation of interatomic decay rates by a combination of the Fano ansatz, Green's-function methods, and the Stieltjes imaging technique. *J. Chem. Phys.* **123,** 204107–204120 (2005).
19. Averbukh, V. & Cederbaum, L. S. Calculation of interatomic decay widths of vacancy states delocalized due to inversion symmetry. *J. Chem. Phys.* **125,** 094107–094114 (2006).
20. Moiseyev, N., Scheit, S. & Cederbaum, L. S. Non-hermitian quantum mechanics: Wave packet propagation on autoionizing potential energy surfaces. *J. Chem. Phys.* **121,** 722–725 (2004).

Author contributions

All authors contributed extensively to the work presented in this paper. N.S., S.S, N.V.K., P.K. and L.S.C. carried out *ab initio* calculations; T.J. carried out the experiment. All authors contributed to the interpretation of results and to the manuscript preparation.

Additional information

The authors declare no competing financial interests. Reprints and permissions information is available online at http://npg.nature.com/reprintsandpermissions. Correspondence and requests for materials should be addressed to L.S.C.